Neurobiology of Disease 87 (2016) 69–79

Contents lists available at ScienceDirect

Neurobiology of Disease

journal homepage: www.elsevier.com/locate/ynbdi

Role of the atypical vesicular glutamate transporter VGLUT3 in L-DOPA-induced dyskinesia

Giuseppe Gangarossa [a,b,c,*], Monica Guzman [d], Vania F. Prado [d], Marco A.M. Prado [d], Stephanie Daumas [e,f,g], Salah El Mestikawy [e,f,g,h,**,1], Emmanuel Valjent [a,b,c,***,1]

[a] CNRS, UMR-5203, Institut de Génomique Fonctionnelle, Montpellier F-34094, France
[b] INSERM, U1191, Montpellier F-34094, France
[c] Université de Montpellier, UMR-5203, Montpellier F-34094, France
[d] Molecular Medicine, Robarts Research Institute, Departments of Physiology and Pharmacology, Anatomy & Cell Biology, The University of Western Ontario, London, Ontario, Canada
[e] INSERM, UMR-S 1130, F-75005 Paris, France
[f] CNRS, UMR 8246, F-75005 Paris, France
[g] Sorbonne Universités, Université Pierre et Marie Curie (UPMC) Paris 06, Institut de Biologie Paris-Seine (IBPS), UM119 Neuroscience Paris Seine, F-75005 Paris, France
[h] Douglas Hospital Research Center, Department of Psychiatry, McGill University, 6875 Boulevard Lasalle Verdun, Quebec, Canada

ARTICLE INFO

Article history:
Received 6 November 2015
Revised 14 December 2015
Accepted 18 December 2015
Available online 19 December 2015

Keywords:
L-DOPA
Dyskinesia
Striatum
Cholinergic interneurons (TANs)
Acetylcholine
Glutamate
Vesicular acetylcholine transporter (VAChT)
Vesicular glutamate transporter type 3 (VGLUT3)
Cell signaling

ABSTRACT

Parkinson's disease (PD) is characterized by the degeneration of dopaminergic neurons. The gold standard therapy relies on dopamine (DA) replacement by the administration of levodopa (L-DOPA). However, with time L-DOPA treatment induces severe motor side effects characterized by abnormal and involuntary movements, or dyskinesia. Although earlier studies point to a role of striatal cholinergic interneurons, also known as striatal tonically active neurons (TANs), in L-DOPA-induced dyskinesia (LID), the underlying mechanisms remain to be fully characterized. Here, we find that DA depletion is accompanied by increased expression of choline acetyltransferase (ChAT), the vesicular acetylcholine transporter (VAChT) as well as the atypical vesicular glutamate transporter type 3 (VGLUT3). TANs number and soma size are not changed. In dyskinetic mice, the VAChT levels remain high whereas the expression of VGLUT3 decreases. LID is attenuated in VGLUT3-deficient mice but not in mice bearing selective inactivation of VAChT in TANs. Finally, the absence of VGLUT3 is accompanied by a reduction of L-DOPA-induced phosphorylation of ERK1/2, ribosomal subunit (rpS6) and GluA1.
Our results reveal that VGLUT3 plays an important role in the development of LID and should be considered as a potential and promising therapeutic target for prevention of LID.

1. Introduction

Parkinson's disease (PD) is a neurodegenerative disorder caused by the progressive loss of dopaminergic neurons innervating the major input structure of the basal ganglia circuit, the striatum (Ehringer and Hornykiewicz, 1960). The classical motor symptoms have been associated with the unbalanced activity of D1R- and D2R-expressing medium-sized spiny projection neurons (MSNs) (Calabresi et al., 2014; Day et al., 2008; Kravitz et al., 2010; Tozzi et al., 2011), which can be restored by the administration of the precursor of dopamine (DA), levodopa (L-DOPA) (Fahn et al., 2004). However, long-term L-DOPA therapy treatment is associated with the development of debilitating motor fluctuations such as abnormal and involuntary movements (AIMs), also known as L-DOPA-induced dyskinesia (LID) (Bastide et al., 2015).

Converging evidence suggest that LID results in part from aberrant striatal MSNs activity (Albin et al., 1989; Bateup et al., 2010; Darmopil et al., 2009; Lindgren et al., 2009; Mallet et al., 2006; Picconi et al., 2003). Indeed, striatal plasticity is strongly altered in dyskinetic animals (Cerovic et al., 2013; Fieblinger et al., 2014a; Picconi et al., 2003; Thiele et al., 2014). Moreover, abnormal activations of intracellular signaling events, including the cAMP/PKA, ERK and mTORC1 pathways have been associated to the development of LID (Heiman et al., 2014; Murer and Moratalla, 2011; Santini et al., 2012, 2007; Westin et al., 2007). In parallel to these changes occurring in the MSNs, several reports suggest that dysregulation of striatal cholinergic interneurons (TANs) could participate to the establishment of abnormal striatal activity associated with LID (DeBoer et al., 1993; Ding et al., 2006; Ding et al., 2011; Fino et al., 2008; Lim et al., 2014). Indeed, following DA

* Correspondence to: G. Gangarossa, CIRB, Collège de France, F-75005, Paris.
** Correspondence to: S. El Mestikawy, INSERM, UMR-S 1130, F-75005 Paris, France.
*** Correspondence to: E. Valjent, INSERM, U1191, Montpellier F-34094, France.
E-mail addresses: peppe.ganga@gmail.com (G. Gangarossa), salah.el_mestikawy@upmc.fr (S. El Mestikawy), emmanuel.valjent@igf.cnrs.fr (E. Valjent).
[1] These authors equally contributed to this work.
Available online on ScienceDirect (www.sciencedirect.com).

http://dx.doi.org/10.1016/j.nbd.2015.12.010
0969-9961/

denervation, the tonic inhibitory control of DA on TANs is lost (Ding et al., 2006; Kayadjanian et al., 1999; Maurice et al., 2004) and repeated administration of L-DOPA leading to dyskinesia enhances striatal cholinergic activity (Ding et al., 2011).

One of the particularities of the TANs is their ability to signal through both acetylcholine (ACh) and glutamate (Gras et al., 2002). Indeed, the co-expression of VAChT and VGLUT3 allows the storage of ACh and glutamate into the same synaptic vesicles (El Mestikawy et al., 2011). The interplay between these two vesicular transporters is functionally important since VGLUT3 inactivation leads to altered efficiency of ACh vesicular filling transport and reduced striatal ACh release (Gras et al., 2008). As a consequence, the lack of VGLUT3 alters the physiology of striatal interneurons and MSNs, thus severely impacting on striatal transmission (Gras et al., 2008; Nelson et al., 2014; Sakae et al., 2015). However, the contributions of ACh and glutamate (released by TANS) for LID are currently unknown. Interestingly, VGLUT3-deficient mice displayed a hypocholinergic phenotype (Gras et al., 2008). Therefore, because of its implication in TANs' functions, and limited expression we hypothesized that VGLUT3 might be a target for the modification of LID.

Here, we demonstrate that DA depletion is accompanied by an increased expression of VAChT and VGLUT3 in hemiparkinsonian mice. In contrast, in dyskinetic mice, while VAChT levels still remain elevated, VGLUT3 expression is strongly decreased in TANs. Moreover, we found that AIMs induced by repeated L-DOPA administration are attenuated in VGLUT3-deficient mice but unaltered in mice lacking VAChT in TANs. Finally, genetic inactivation of VGLUT3 reduced the phosphorylation of ERK1/2, ribosomal protein S6 and GluA1, molecular markers of LID. Together, our results indicate that VGLUT3 is critically involved in the development of LID.

2. Materials and methods

2.1. Animals

Male 10–16 weeks old mice were used and maintained in a 12 h light/dark cycle, in stable conditions of temperature (22 °C) and humidity (60%), with food and water ad libitum. All experiments were in accordance with the guidelines of the French Agriculture and Forestry Ministry for handling animals (authorization number/license D34-172-13). C57BL/6J mice were purchased from Charles Rivers (France). VGLUT3 knockout mouse line was backcrossed on a C57BL6/J background for 10 generations (as previously described, (Sakae et al., 2015). *Drd2-Cre*::$VAChT^{loxP/loxP}$ mice were generated by crossing $VAChT^{loxP/loxP}$ with the D2-Cre mouse line and have been backcrossed 4 generations to C57BL6/J (Guzman et al., 2011). All procedures were approved by the local animal care committee (University of Western Ontario Protocol 2008-127) and followed guidelines of Canadian Council for Animal Care.

2.2. Drugs

L-DOPA (Sigma-Aldrich) was injected at a dose of 10 mg/kg in combination with the peripheral DOPA decarboxylase inhibitor, benserazide hydrochloride (Sigma-Aldrich) (7.5 mg/kg). Both drugs were dissolved in saline (0.9% NaCl) and injected intraperitoneally in a total volume of 10 ml/kg body weight. When mice were not treated with L-DOPA, they received an equivalent volume of vehicle. Desipramine hydrochloride (Tocris), injected at a dose of 20 mg/kg, was dissolved in saline (0.9% NaCl) and injected intraperitoneally 30 min before 6-OHDA microinjections.

2.3. 6-OHDA lesions

Mice were anesthetized with a mixture of ketamine and xylazine and mounted in a stereotaxic frame (David Kopf Instruments, Tujunga, CA) equipped with a mouse adaptor. 6-OHDA-HCl (Sigma) was dissolved in 0.02% ascorbic acid in saline at a concentration of 3 μg of free-base 6-OHDA/μl. Each mouse received two unilateral injections of 6-OHDA (2 μl/injection) into the right dorsal striatum as described previously (Francardo et al., 2011; Santini et al., 2007), according to the following coordinates (in mm): anterior–posterior +1, medial–lateral −2.1, dorsal–ventral −3.2 and anterior–posterior +0.3, medial–lateral −2.3, and dorsal–ventral −3.2 (Franklin and Paxinos, 2007). Before 6-OHDA microinjections, all the mice received a pre-treatment with desipramine to prevent noradrenergic degeneration (Fulceri et al., 2006). Mice were allowed to recover for 3 weeks before drug treatment and behavioral evaluation. This procedure leads to a decrease in striatal tyrosine hydroxylase immunoreactivity ≥80% (Supplemental Fig. 1) and to a marked akinesia affecting the side of the body contralateral to the lesioned striatum. Post-operative caring was performed as previously described (Francardo et al., 2011).

2.4. Spontaneous locomotor activity

Locomotor activity was measured as described (Gangarossa et al., 2013). Horizontal activity and rearings were measured in a circular corridor (Imetronic, Pessac, France). Counts for horizontal activity were incremented by consecutive interruption of two adjacent beams placed at a height of 1 cm per 90° sector of the corridor (mice moving through one-quarter of the circular corridor) and counts for vertical activity (rearing) as interruption of beams placed at a height of 7.5 cm along the corridor (mice stretching upwards). All mice were placed for 60 min in the activity box.

2.5. Cylinder test

The cylinder test was performed as previously described (Espadas et al., 2012) 3 weeks after 6-OHDA lesion and on day 5 of chronic L-DOPA treatment, 140 min after L-DOPA injection to avoid dyskinetic symptoms (Lundblad et al., 2002; Picconi et al., 2003). Spontaneous ipsilateral and contralateral forelimb touches to the cylinder walls were counted for 3–5 min to assess forelimb asymmetry and expressed as percentage of use as in Lundblad et al. (2002).

2.6. Motor coordination

Motor coordination was measured using a mouse accelerating rotarod (Ugo Basile, Comerio, Italy) following an accelerating protocol, with increasing speed from 4 to 40 rpm over a 5-min period as described (Gangarossa et al., 2014b). Mice were tested in three consecutive trials. Measurements were done before injection of 6-OHDA (naive); 3 weeks after lesion (Parkinsonian); and after L-DOPA treatment, hours after the L-DOPA injection to avoid exhaustion and the peak dyskinesia.

2.7. Abnormal and involuntary movements (AIMs)

Mice were treated for 12 consecutive days with 1 injection per day of L-DOPA (10 mg/kg) plus benserazide (7.5 mg/kg). AIMs were assessed after the L-DOPA injection (day 6 and day 12) using a previously established scale (Cenci et al., 1998; Lundblad et al., 2002, 2004; Pavon et al., 2006). 20 min after L-DOPA administration, mice were placed in separate cages, and individual dyskinetic behaviors (i.e. AIMs) were assessed for 1 min every 20 min over a period of 120 min. AIMs were classified into four subtypes as follows: locomotor AIMs (contralateral turns), axial AIMs (dystonic posturing of the upper part of the body toward the side contralateral to the lesion), limb AIMs (abnormal movements of the forelimb contralateral to the lesion), and orolingual AIMs (vacuous jaw movements and tongue protrusion). Each subtype was scored on a severity scale from 0 to 4 as follows: 0,

absent; 1, occasional; 2, frequent; 3, continuous; 4, continuous and not interruptible by outer stimuli.

2.8. Tissue preparation and immunofluorescence

Mice were rapidly anesthetized with pentobarbital (500 mg/kg, i.p., Sanofi-Aventis, France) and transcardially perfused with 4% (weight/vol.) paraformaldehyde in 0.1 M sodium phosphate buffer (pH 7.5). Brains were post-fixed overnight in the same solution and stored at 4 °C. Sections (30 μm) were cut with a vibratome (Leica, France) and stored at −20 °C in a solution containing 30% (vol/vol) ethylene glycol, 30% (vol/vol) glycerol and 0.1 M sodium phosphate buffer, until they were processed for immunofluorescence. Sections were processed as follows: day 1: free-floating sections were rinsed in Tris-buffered saline (TBS; 50 mM Tris–HCL, 150 mM NaCl, pH 7.5), incubated for 5 min in TBS containing 3% H_2O_2 and 10% methanol, and then rinsed three times for 10 min each in TBS. After 15 min incubation in 0.2% Triton X-100 in TBS, sections were rinsed three times in TBS again. Finally, they were incubated overnight at 4 °C with the different primary antibodies. Slices were then incubated overnight or 72 h at 4 °C with the following primary antibodies: mouse anti-TH (1:1000, Millipore, MAB318), rabbit anti-VAChT (1:500, Synaptic System, #139103), guinea-pig anti-VGLUT3 (home-made 1:500, (Gras et al., 2008) and goat anti-ChAT (1:1000, Millipore, AB144P). Sections were rinsed three times for 10 min in TBS and incubated for 45 min with goat Cy2-, Cy3- and Cy5-coupled (1:500, Jackson Lab) and/or goat A488 (1:500, Invitrogen). Sections were rinsed for 10 min twice in TBS and twice in Tris-buffer (1 M, pH 7.5) before mounting in 1,4-diazabicyclo-[2.2.2]-octane (DABCO, Sigma-Aldrich).

Confocal microscopy and image analysis were carried out at the RIO Imaging Facility (Montpellier, France). Images were acquired using sequential laser scanning confocal microscopy (Zeiss LSM780) with the following band-pass and long-pass filter setting: Alexa 488 (band pass filter: 505–530), Cy3 (band pass filter: 560–615) and Cy5 (long-pass filter 650). Each confocal plan (212.55 μm × 212.55 μm) obtained with the ×40/1.3 oil-immersion lens was generated as merge of two channels. The objectives and the pinhole setting (1 airy unit) remain unchanged during the acquisition of all images. Quantification of immunofluorescence intensity within a given region of interest (ROIs) was performed using the analysis/measure plugin of the ImageJ software taking as standard reference a fixed threshold of fluorescence. Only $ChAT^+$/$VAChT^+$/$VGLUT3^+$ interneurons in which the cell soma was clearly represented were considered as appropriate ROIs for densitometric analysis. To avoid contamination and false positive signals for cellular compartment analyses, $ChAT^+$/$VAChT^+$/$VGLUT3^+$ interneurons were considered as appropriate when the cytoplasmic signal was clearly distinguishable from the nucleus in order to virtually set the focal plan inside the quantified neuron, thus minimizing artifacts and signal contaminations (e.g. ceiling or floor effects).

2.9. Western blotting

Western blotting experiments were performed as previously described (Gangarossa et al., 2014a; Gangarossa and Valjent, 2012). In brief, mice were sacrificed by decapitation. The heads of the animals were then immersed in liquid nitrogen for 5 s. The brains were quickly removed and the striata dissected out on ice-cold surface, sonicated in 350 μl of 1% SDS and boiled for 10 min. Aliquots (2.5 μl) of the homogenate were used for protein determination using a BCA assay kit (Pierce Europe). Equal amounts of proteins (15 μg) for each sample were loaded onto 8% polyacrylamide gels. Proteins were separated by SDS-PAGE and transferred to PVDF membranes (GE Healthcare). The membranes were immunoblotted using tyrosine hydroxylase (1:2000; Millipore, MAB318), pT202/Y204/T185/Y187-ERK1/2 (1:2000; Cell Signaling, #9101), ERK1/2 (1:2000; Cell Signaling, #4695), pS235/236-rpS6 (1:2000; Cell Signaling, #2211), pS240/244-rpS6 (1:2000; Cell Signaling, #2215), rpS6 (1:1000; Cell Signaling, #2317), pS845-GluA1 (1:1000; Millipore, #04–1073), GluA1 (1:750; Millipore, AB1504) and β-actin (1:40,000; Abcam, ab6276) antibodies. Bound antibodies were detected with HRP-conjugated anti-rabbit or anti-mouse antibodies (1:10,000; Cell Signaling Technology) and visualized by enhanced chemiluminescence detection. Quantifications were performed using ImageJ.

2.10. Statistical analysis

All the data were analyzed using one-way ANOVA followed by Newman–Keuls *post-hoc* test or two-way ANOVA followed by Bonferroni *post hoc* test. Unpaired Student's *t*-test was used when necessary. In all cases, significance threshold was set at $p < 0.05$. Prism 6.0 software (GraphPad) was used to perform statistical analyses. Results are expressed as mean ± SEM.

3. Results

3.1. DA depletion and L-DOPA treatment do not alter the number of TANs

Dysregulations of TANs have been reported in rodent models of Parkinson's disease (Pisani et al., 2003). To determine the impact of DA depletion on TANs, we first analyzed whether the number of TANs was altered in 6-OHDA-lesioned mice. The quantification of the number ChAT-positive interneurons in both dorsomedial and dorsolateral striatum revealed no differences in the DA-depleted side compared to the unlesioned side (Fig. 1a, b). In addition no change in the TANs soma size was observed (Fig. 1c).

To test whether LID was accompanied with an altered number of TANs, 6-OHDA-lesioned mice were treated once a day with L-DOPA (10 mg/kg) (in combination with 7.5 mg/kg of benserazide to prevent the conversion of L-DOPA to DA at the periphery) for 12 consecutive days. The number of ChAT-positive interneurons as well as the some size of TANs remained unchanged in dyskinetic mice (Fig 1d–f). Altogether these data revealed that DA depletion and L-DOPA treatment do not alter the number and the size of TANs.

3.2. Increased striatal expression of ChAT, VAChT and VGLUT3 in 6-OHDA-lesioned mice

We next examined whether DA-depletion was accompanied by changes in striatal expression levels of ChAT. Whereas the intensity of ChAT was unchanged at the somatic level, an increase of ChAT expression (30 ± 4%, $p < 0.001$) was observed at the level of the neuropil in the striatal lesioned side compared to the unlesioned side (Fig. 2a, b).

TANs co-express VAChT and VGLUT3 (El Mestikawy et al., 2011). We next investigated whether changes in the expression levels of these two transporters occurred in 6-OHDA-lesioned mice. As observed with ChAT, the expression of VAChT and VGLUT3 was increased selectively in the neuropil (29 ± 3.1% and 14 ± 2.5%, respectively) in the 6-OHDA-lesioned side compared to the unlesioned striatum (Fig. 2c–e). Altogether these results revealed that DA-depletion is accompanied by an enhanced striatal expression of several markers of TANs.

3.3. Differential regulation of ChAT, VAChT and VGLUT3 expressions in dyskinetic mice

ChAT, VAChT and VGLUT3 levels were then analyzed in mice developing dyskinesia. In lesioned mice, the increase of ChAT levels in the striatal neuropil returned to basal levels following 12 days of treatment with L-DOPA (Fig. 3a, b) while the enhanced level of VAChT persisted (Fig. 3c, d). In contrast, VGLUT3 levels were decreased in dyskinetic mice (Fig. 3c, e). Indeed, in addition to the normalization of VGLUT3 levels in the striatal neuropil, we observed a decrease (~25 ± 2.3%, $p < 0.001$) in the intensity of VGLUT3 staining in the soma of TANs

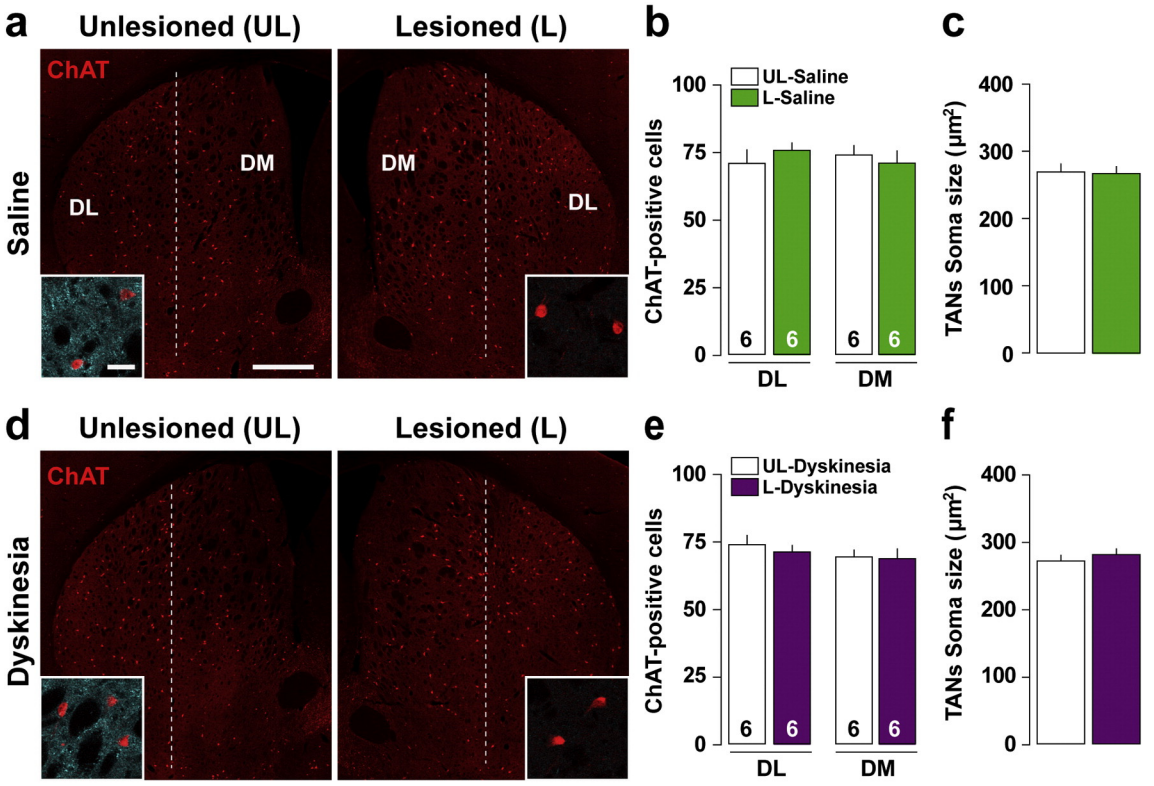

Fig. 1. TANs number in DA-denervated and dyskinetic mice. Immunofluorescence detection (**a**) and quantification (**b**) of ChAT-positive interneurons in the unlesioned (UL) and lesioned (L) dorsomedial (DM) and dorsolateral (DL) striatum of saline-treated mice. Scale bar: 500 µm. (n = 6 mice per group). Student's *t*-test: $p > 0.5$, ns. Insets show ChAT (red) and TH (cyan) immunolabelings. Scale bar: 50 µm. (**c**) Measure of TANs soma size in the unlesioned and lesioned striatum of saline-treated mice (37–39 pictures from 6 mice per group). Student's *t*-test $p > 0.5$, ns. Immunofluorescence detection (**d**) and quantification (**e**) of ChAT-positive interneurons in the unlesioned (UL) and lesioned (L) dorsomedial (DM) and dorsolateral (DL) striatum of L-DOPA-treated mice (dyskinesia) (n = 6 mice per group). Student's *t*-test: $p > 0.5$, ns. Insets (**D_1** and **D_2**) show ChAT (red) and TH (cyan) immunolabelings. (**f**) Measure of TANs soma size in the unlesioned and lesioned striatum of dyskinetic mice (37–39 pictures from 6 mice per group). Student's *t*-test $p > 0.5$, ns.

(Fig. 3c, e). These changes were specific of the dopamine-depleted striatum since no differences in VAChT and VGLUT3 levels were detected in the unlesioned striata of both saline- and L-DOPA-treated mice (Supplemental Fig. 2). Altogether, these data suggest that L-DOPA-induced dyskinesia is accompanied by opposite dysregulation of VAChT and VGLUT3 levels within the striatum.

3.4. Motor impairment induced by DA depletion and antiparkinsonian properties of L-DOPA are preserved in VGLUT3-deficient mice

To investigate whether VGLUT3 participates to the motor impairment observed following DA depletion we used VGLUT3-deficient mice and their wild-type littermates. To rule any potential motor dysfunctions in the mutant mice that may interfere with the effects of the lesioned and the subsequent treatment with L-DOPA, spontaneous locomotor activity and motor coordination were evaluated in both wild-type and VGLUT3-deficient mice. No difference in spontaneous horizontal locomotor activity was observed between both genotypes (Fig. 4a, b). In contrast, VGLUT3 knockout mice displayed a significant reduction in the number of rearings (Fig. 4c). This reduced vertical locomotor activity was not due to motor coordination impairment since no differences were found between genotypes in the rotarod test (Fig. 4d).

WT and VGLUT3-deficient mice were next lesioned unilaterally with 6-OHDA and tested for spontaneous rotations and motor coordination 3 weeks later. The impaired motor coordination induced by DA depletion was indistinguishable in both genotypes and L-DOPA treatment improved motor performance in a similar manner in both genotypes (Fig. 4d). Moreover, no differences were observed in the number of spontaneous ipsilateral rotations suggesting that the two groups of mice displayed similar body asymmetry (Fig. 4e).

To test whether VGLUT3 inactivation interfered with akinesia, the cylinder test was performed 3 weeks after the lesion in WT and VGLUT3-deficient mice. Mice lacking VGLUT3 performed less rearings and wall contacts (Fig. 4f). However, striatal unilateral 6-OHDA lesion resulted in akinesia (as demonstrated by the decrease in the use of the contralateral forelimb) in both VGLUT3 knockout and WT mice (Fig. 4g). Moreover, the reversion of forelimb akinesia was identical in the two groups of mice following the acute administration of L-DOPA (10 mg/kg) (Fig. 4g), thus suggesting that the therapeutic effect of L-DOPA was maintained in the absence of VGLUT3. Together, our results reveal that VGLUT3 inactivation neither affects motor impairment induced by DA depletion nor interferes with the antiparkinsonian properties of L-DOPA.

3.5. LID is attenuated in VGLUT3-deficient mice

We next investigated the involvement of VGLUT3 in the development of abnormal and involuntary movements. WT and VGLUT3-deficient mice unilaterally lesioned with 6-OHDA were treated daily with L-DOPA (10 mg/kg). AIMs, including locomotor, axial dystonia, forelimb and orofacial dyskinesia, were evaluated after of L-DOPA injection during 120 min on day 6 and day 12. In WT mice, repeated administration of L-DOPA induced severe dyskinetic responses at day 12 (Fig. 5a) which peaked at 60 min and gradually declined at 120 min (Fig. 5b). On the other hand, LID was strongly attenuated in mice lacking VGLUT3 (Fig. 5a–c). Moreover, the analysis of each individual AIMs revealed that the four AIMs subscores were reduced in VGLUT3-

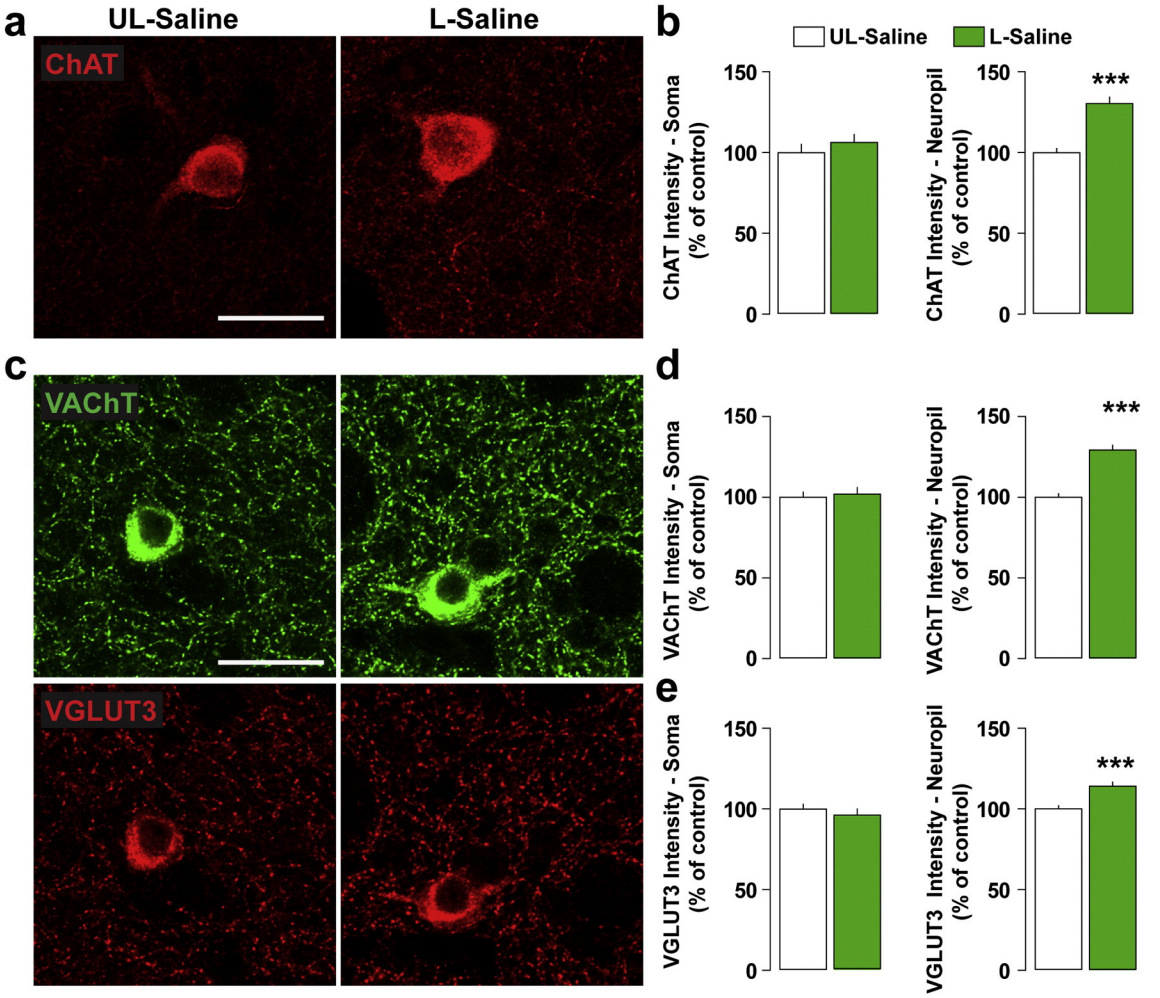

Fig. 2. Expression level of ChAT, VAChT and VGLUT3 in DA-depleted mice. (**a**) Immunofluorescence detection of ChAT-positive interneurons in the unlesioned and lesioned striatum of saline-treated mice. Scale bar: 40 μm. (**b**) Measurement of ChAT intensity in the soma and neuropil in the unlesioned and lesioned striatum of saline-treated mice. Student's *t*-test: (37–39 pictures from 6 mice per group) ***$p < 0.001$. (**c**) Immunofluorescence detection of VAChT and VGLUT3 in the unlesioned and lesioned striatum of saline-treated mice. Scale bar: 40 μm. (**d** and **e**) Measurement of VAChT (**d**) and VGLUT3 (**e**) intensity in the soma (62–69 interneurons from 7 mice per group) and neuropil (55–56 pictures from 7 mice per group) in the unlesioned and lesioned striatum of saline-treated mice. Student's *t*-test: ***$p < 0.001$.

deficient mice (Fig. 5d–g). Importantly, the effects observed were not linked to the extent of DA depletion between the two genotypes since no difference in the remaining striatal TH level was found (WT: 11 ± 1.9%, VGLUT3 knockout 12 ± 3.6%, $p < 0.001$).

TANs co-express VGLUT3 and VAChT (Gras et al., 2008). To investigate whether VAChT was involved in the development LID, AIMs were evaluated in mice lacking VAChT in TANs (*Drd2-Cre*::*VAChT*$^{LoxP/LoxP}$, (Guzman et al., 2011). *Drd2-Cre*::*VAChT*$^{LoxP/LoxP}$ and *VAChT*$^{LoxP/LoxP}$ mice unilaterally lesioned with 6-OHDA were daily treated with L-DOPA for 12 consecutive days. In contrast to what we observed with VGLUT3-deficient mice, LID was more sever at day 6 in mice lacking VAChT in TANs compared to their WT littermates (Fig. 6a). However, following 12 days of L-DOPA treatment the expression of LID was indistinguishable in WT and VAChT cKO (Fig. 6a–g). Together, these results indicate that VGLUT3 is involved in the development of LID.

3.6. L-DOPA-induced phosphorylation of ERK, ribosomal protein S6 and GluA1 is attenuated in VGLUT3-deficient mice

Exacerbated activation of several intracellular signaling pathways has been causally associated with the development of LID (Bastide et al., 2015). To investigate the consequence of VGLUT3 deficiency on L-DOPA-induced aberrant signaling within the striatum, WT and VGLUT3 knockout mice were sacrificed 30 min after a last injection of L-DOPA and striatal levels of phosphorylated ERK1/2, ribosomal protein S6 (rpS6) and GluA1, a subunit of the glutamate AMPA receptor, were assessed by Western blot. In WT lesioned mice, L-DOPA enhanced the phosphorylation of ERK1/2 (Fig. 7a, b), rpS6 at both sites S235/236 and S240/244 (Fig. 7c, d) and GluA1 at S845 (Fig. 7e). These L-DOPA-induced phosphorylations were significantly reduced in the lesioned striatum of VGLUT3-deficient mice compared to WT animals (Fig. 7a–e). In contrast, no differences of the abovementioned phospho-proteins were detected in the unlesioned striatum of mutant and WT mice (Fig. 7). Together these results indicate that attenuation of LID in VGLUT3-deficient mice is accompanied by a reduction of the ability of L-DOPA to exacerbate striatal signaling.

4. Discussion

Striatal cholinergic interneurons play a critical role in shaping and controlling the activity of the striatum. Increasing evidences associate TANS dysregulation with several striatum-related disorders including PD (Bonsi et al., 2011; Deffains and Bergman, 2015; Ding et al., 2011; Girasole and Nelson, 2015; Pisani et al., 2007; Won et al., 2014). In DA-depleted animals, the autonomous pacemaking activity of TANs is strongly altered (Bennett and Wilson, 1999; Calabresi et al., 2006; Ding

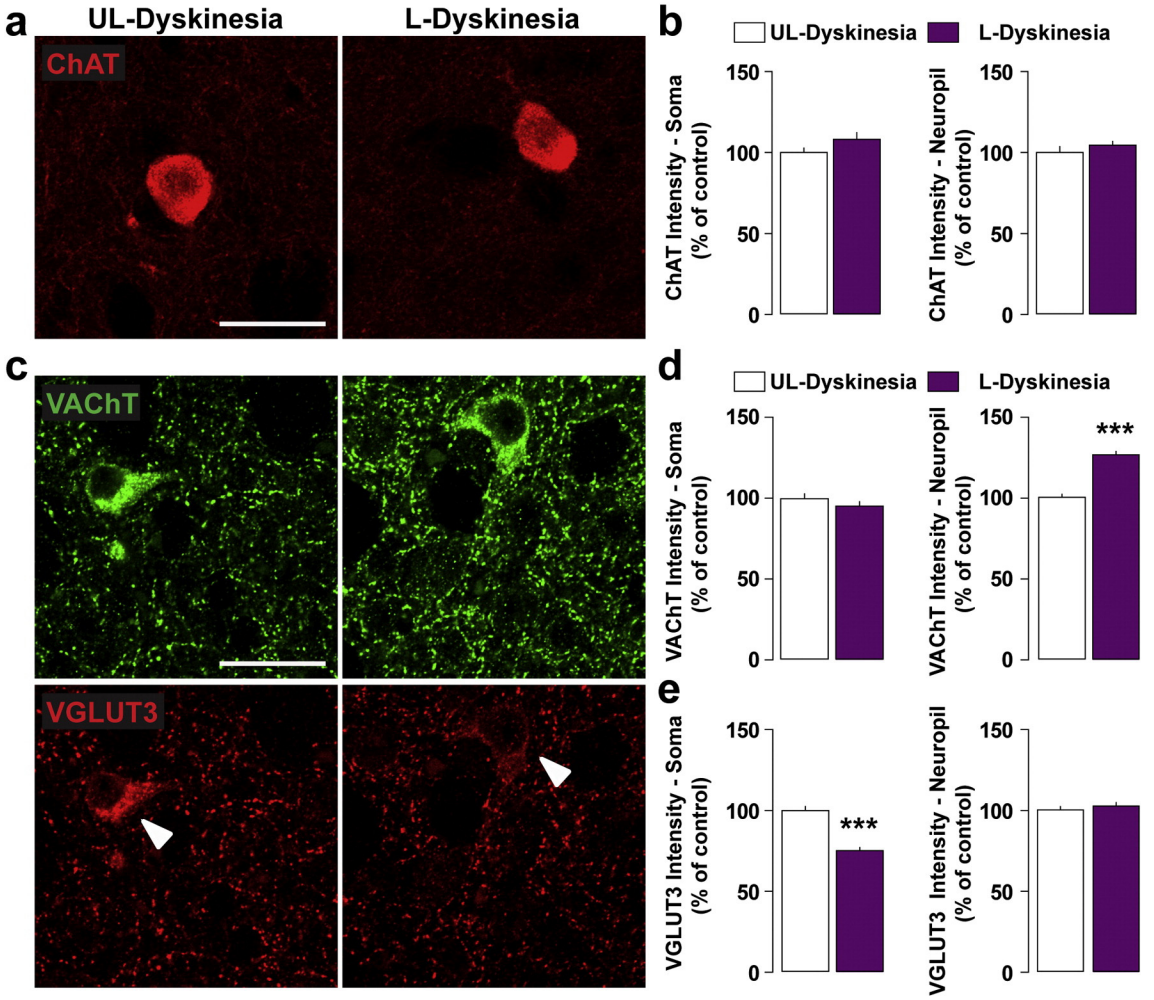

Fig. 3. Expression levels of ChAT, VAChT and VGLUT3 in dyskinetic mice. (**a**) Immunofluorescence detection of ChAT-positive interneurons in the unlesioned and lesioned striatum of dyskinetic mice. Scale bar: 40 μm. (**b**) Measurement of ChAT intensity in the soma and neuropil in the unlesioned and lesioned striatum of saline-treated mice. Student's *t*-test: (38–40 pictures from 6 mice per group) $p > 0.5$, ns. (**c**) Immunofluorescence detection of VAChT and VGLUT3 in the unlesioned and lesioned striatum of saline-treated mice. Scale bar: 40 μm. (**d** and **e**) Measurement of VAChT (**d**) and VGLUT3 (**e**) intensity in the soma (67–72 interneurons from 7 mice per group) and neuropil (62–69 pictures from 7 mice per group) in the unlesioned and lesioned striatum of saline-treated mice. Student's *t*-test: $^{***}p < 0.001$.

et al., 2006). Indeed, loss of the tonic inhibitory control exerted by DA through D2R has been proposed to contribute to the hypercholinergia observed in animal models of PD (Calabresi et al., 2006; Centonze et al., 2003; Chuhma et al., 2014; Tozzi et al., 2011). However, the fact that TANs not only signal with ACh, but also with glutamate, has rarely been taken into consideration in the context of experimental Parkinsonism. Given the critical role of VAChT and VGLUT3 in the signaling activity of TANs, it is tempting to speculate that the increased levels of these two vesicular transporters observed after DA denervation constitutes one of the adaptive mechanisms taking place after the loss of D2R inhibition. Whether transcriptional or/and post-transcriptional mechanisms are involved in the increase VAChT and VGLUT3 levels remain to be determined.

Exacerbated activity of TANs has also been associated with L-DOPA-induced dyskinesia (Ding et al., 2011). Indeed, pharmacological reduction of ACh tone or TANs ablation attenuates the expression and the development of LID, respectively (Ding et al., 2011; Won et al., 2014). Whereas the loss of DA transmission leads to increased VAChT and VGLUT3 levels in the striatum, only VGLUT3 levels are downregulated following the restoration of DA transmission by L-DOPA treatment. This decrease may be the result of a homeostatic response to counterbalance the hypercholinergic tone triggered by DA loss.

The increased VGLUT3 level in DA-depleted striatum and its normalization following L-DOPA treatment led us to hypothesize that VGLUT3 regulation may participate in the genesis of dyskinesia in PD by modulating TANs. Supporting this hypothesis, LID is strongly attenuated in VGLUT3-deficient mice (present study and (Divito et al., 2015)). In this later study, Parkinsonian symptoms were also attenuated in VGLUT3 deficient mice (Divito et al., 2015), an effect we did not observed (present study). These differences may be caused by the different methodological lesion approaches used in the two studies. In contrast, AIMs induced by chronic administration of L-DOPA (12 days) are unaltered in mice lacking VAChT selectively in TANs. However, we noticed that at day 6, LID was more pronounced in VAChT conditional knockout mice suggesting that these mice could be more sensitive to L-DOPA. Interestingly, selective deletion of VAChT in TANs lead to compensatory mechanisms including changes in muscarinic M4R and dopamine D1R and D2R as well as increased response to D1R agonist (Guzman et al., 2011). Whether D1R hyperactivity previously observed (Guzman et al., 2011) compensate for the lack of Ach and therefore sustain LID in VAChT conditional knockout mice will require further investigations.

Our result suggests that the reduction of LID consequent to VGLUT3 deletion was likely caused by the absence of glutamate release rather than by a reduction of ACh tone (Cachope et al., 2012; Higley et al., 2011; Nelson et al., 2014). Similar dichotomy between ACh and VGLUT3-dependent glutamate has been reported in other striatal-related disorders, such as addiction (Guzman et al., 2011; Sakae et al., 2015). Indeed, VGLUT3 knockout mice display an enhanced sensitivity

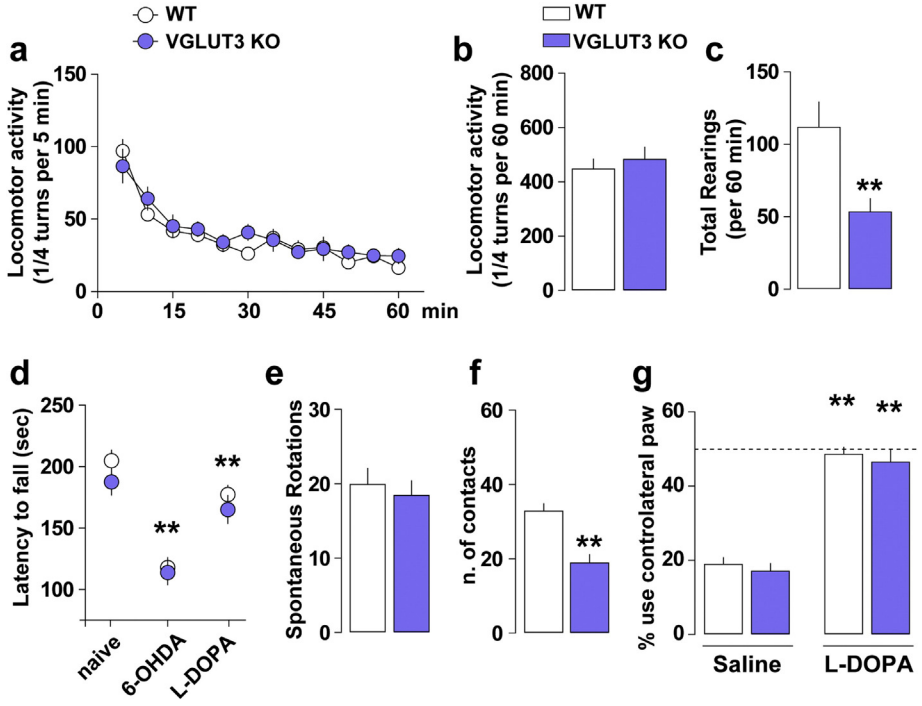

Fig. 4. Antiparkinsonian properties of L-DOPA are preserved in VGLUT3-deficient mice. (**a**) Horizontal locomotor activity of VGLUT3 KO (n = 9) and WT mice (n = 12) in a novel non-stressful environment. Data were analyzed using two-way ANOVA: (Time × Genotype: $F_{(11, 209)} = 0.94$, p = 0.50; Time: $F_{(11, 209)} = 32.58$, $p < 0.001$; Genotype: $F_{(1, 209)} = 0.39$, p = 0.54). (**b**) Cumulative horizontal locomotor activity of WT and VGLUT3 KO mice over a 60 min period. Data were analyzed using Student's *t*-test: $p > 0.5$, ns. (**c**) Number of rearings in WT and VGLUT3 KO mice over a 60 min period. Data were analyzed using Student's *t*-test: $^{**}p < 0.01$. (**d**) Motor coordination in VGLUT3 KO (n = 9) and WT (n = 12) mice before injection of 6-OHDA (naïve); 3 weeks after lesion (Parkinsonian); and after L-DOPA treatment. Data (means ± SEM) were analyzed using two-way ANOVA: (Time × Genotype: $F_{(2, 54)} = 0.26$, p = 0.77; Time: $F_{(2, 54)} = 58.09$, $p < 0.001$; Genotype: $F_{(1, 54)} = 2.14$, p = 0.15). (**e**) Ipsilateral spontaneous rotation in VGLUT3 KO and WT mice. Data were analyzed using Student's *t*-test: $p > 0.5$, ns. (**f**) Number of wall touches in the cylinder test. Data were analyzed using Student's *t*-test: $^{**}p < 0.01$. (**g**) Forelimb asymmetry of VGLUT3 KO (n = 9) and WT (n = 12) mice 3 weeks after lesion (Parkinsonian) and after L-DOPA treatment. Data were analyzed using two-way ANOVA: (Time × Genotype: $F_{(1, 38)} = 0.02$, p = 0.96; Time: $F_{(1, 38)} = 170.02$, $p < 0.001$; Genotype: $F_{(1, 38)} = 0.75$, p = 0.39).

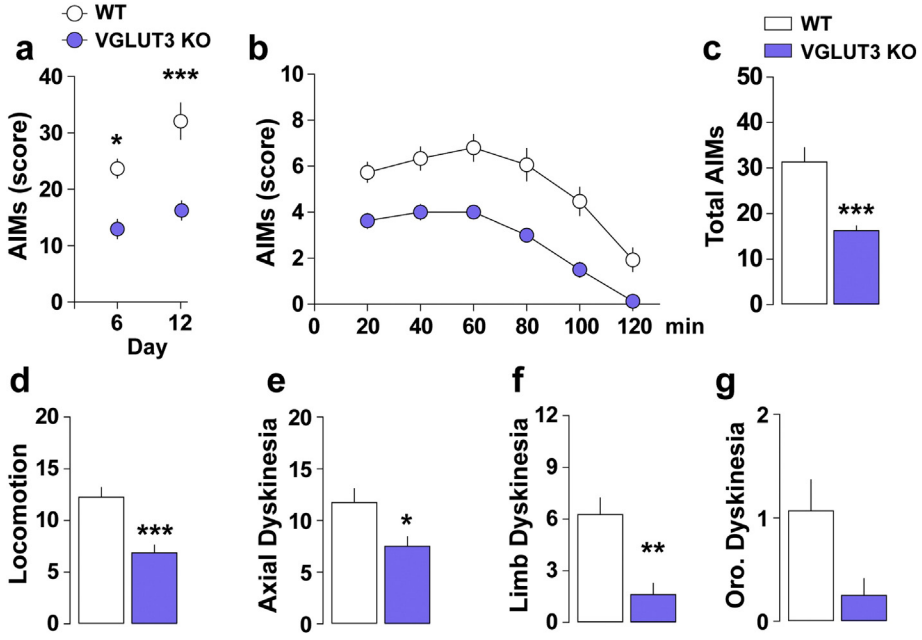

Fig. 5. LID is attenuated in VGLUT3-deficient mice. (**a**) Time course of total abnormal and involuntary movements (AIMs) scored at day 6 and day 12. Data were analyzed using two-way ANOVA: (Time × Genotype: $F_{(1, 38)} = 2.95$, p = 0.09; Time: $F_{(1, 38)} = 2.66$, p = 0.11; Genotype: $F_{(1, 38)} = 24.88$, $^{***}p < 0.001$). Bonferroni *post-hoc* test was used for specific comparisons: $^{*}p < 0.05$ (VGLUT3 KO-day6 vs WT-day6) and $^{***}p < 0.001$ (VGLUT3 KO-day12 vs WT-day12). (**b**) Time course of total AIMs scored every 20 min over a period of 120 min in VGLUT3 KO (n = 9) and WT mice (n = 12) following the last injection of L-DOPA. Data were analyzed using two-way ANOVA: (Time × Genotype: $F_{(5, 95)} = 2.08$, p = 0.07; Time: $F_{(5, 95)} = 90.31$, $^{***}p < 0.001$; Genotype: $F_{(1, 95)} = 27.05$, $^{**}p < 0.01$). (**c**) Cumulative AIMs in VGLUT3 KO and WT mice. Data were analyzed using Student's *t*-test: $^{***}p < 0.001$. (**d**) Cumulative locomotor dyskinesia in both genotypes. Student's *t*-test: $^{***}p < 0.001$. (**e**) Cumulative axial dyskinesia in both genotypes. Student's *t*-test: $^{*}p < 0.05$. (**f**) Cumulative limb dyskinesia in both genotypes. Student's *t*-test: $^{**}p < 0.01$. (**g**) Cumulative orofacial dyskinesia in both genotypes. Student's *t*-test: $p > 0.05$, ns.

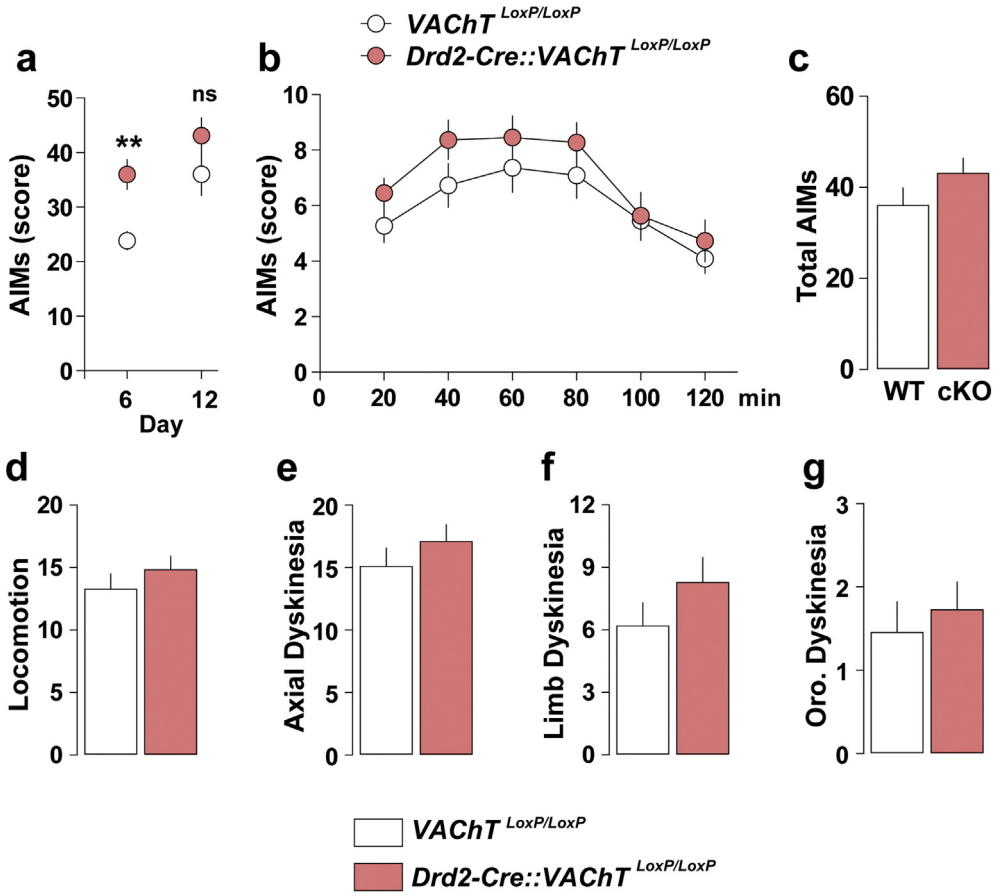

Fig. 6. LID is unchanged in *Drd2-Cre*::*VAChT*$^{LoxP/loxP}$ mice. (**a**) Time course of total abnormal and involuntary movements (AIMs) scored at day 6 and day 12. Data were analyzed using two-way ANOVA: (Time × Genotype: $F_{(1, 40)} = 1.75$, $p = 0.19$; Time: $F_{(1, 40)} = 11.72$, $^{**}p < 0.01$; Genotype: $F_{(1, 40)} = 13.70$, $^{***}p < 0.001$). Bonferroni *post-hoc* test was used for specific comparisons: $^{**}p < 0.01$ (VAChT cKO-day6 vs WT-day6). (**b**) Time course of total AIMs scored every 20 min over a period of 120 min in *Drd2-Cre*::*VAChT*$^{LoxP/loxP}$ (n = 11) and *VAChT*$^{LoxP/loxP}$ mice (n = 11) following the last administration of L-DOPA (day 12). Data were analyzed using two-way ANOVA: (Time × Genotype: $F_{(5, 100)} = 0.73$, $p = 0.60$; Time: $F_{(5, 100)} = 23.22$, $^{***}p < 0.001$; Genotype: $F_{(1, 100)} = 1.26$, $p = 0.27$). (**c**) Cumulative AIMs scored during 120 min. Data were analyzed using Student's *t*-test: $p > 0.05$, ns. (**d**) Cumulative locomotor dyskinesia in both genotypes. Student's t-test: $p > 0.05$, ns. (**e**) Cumulative axial dyskinesia in both genotypes. Student's *t*-test: $p > 0.05$, ns. (**f**) Cumulative limb dyskinesia in both genotypes. Student's t-test: $p > 0.05$, ns. (**g**) Cumulative orofacial dyskinesia in both genotypes. Student's *t*-test: $p > 0.05$, ns.

to locomotor effects of cocaine whereas VAChT conditional knockout mice do not (Gras et al., 2008; Guzman et al., 2011; Sakae et al., 2015). Moreover, it seems that whereas the absence of VGLUT3 increases dopamine release, the absence of VAChT decreases dopamine release, suggesting bidirectional regulation of dopamine by TANs (Sakae et al., 2015). Interestingly, glutamate released from TANs influence striatal activity through activation of mGluRs (Sakae et al., 2015). Given the role played by mGluR5 in the development of LID (Bezard et al., 2014; Fieblinger et al., 2014b; Iderberg et al., 2013; Morin et al., 2014; Morin et al., 2013; Ouattara et al., 2011; Picconi and Calabresi, 2014), it is tempting to hypothesize that abnormal glutamate release from TANs following DA depletion may participate to the development and severity of dyskinesia.

However it is worth to mention that in addition to the TANs, VGLUT3 is also expressed in other non-glutamatergic neurons throughout the brain (El Mestikawy et al., 2011; Herzog et al., 2004; Stensrud et al., 2013). Among them, VGLUT3 is found in the 5-HT terminals arising from the raphe nuclei (Gagnon and Parent, 2013; Herzog et al., 2004). As for ACh in TANs, VGLUT3 also critically regulates the vesicular loading of 5-HT (Amilhon et al., 2010). Importantly, within the striatum more than 75% of VGLUT3 is present in ACh varicosities and 3D reconstruction helped to establish that the remaining 25% are localized in 5-HT fibers (Sakae et al., 2015). Striatal 5-HT transmission is strongly altered in PD and increasing evidences reveal its critical role in the development of LID (Bezard and Carta, 2015; Carta et al., 2007, 2010; Cenci, 2014; Kannari et al., 2001; Nahimi et al., 2012; Rylander et al., 2010). Therefore, it cannot be excluded that the absence of VGLUT3 from the serotonergic terminals innervating the striatum may contribute to the attenuation of LID observed in VGLUT3-deficient mice. Future studies will be necessary to assess the specific role of VGLUT3 in TANs and 5-HT fibers in the development of LID.

In parallel to the attenuation of LID, VGLUT3-deficient mice display a reduction of the phosphorylation of ERK1/2 and rpS6, a downstream target of mTORC1 pathway, two signaling cascades known to be causally linked to the development of LID (Bateup et al., 2010; Fieblinger et al., 2014b; Santini et al., 2012; Santini et al., 2007; Westin et al., 2007). While their contribution in the pathogenesis of LID has been largely attributed to their aberrant activation in D1R-expressing MSNs (Feyder et al., 2011), several lines of evidence suggest that abnormal regulation of these two signaling pathways within TANs could also contribute to the development of dyskinesia. Indeed, increased ERK and rpS6 phosphorylation have been observed in TANs in dyskinetic mice (Ding et al., 2011; Santini et al., 2009a, 2009b). Furthermore, the blockade of ERK pathway reduced TANs hyperactivity induced by repeated L-DOPA treatment (Ding et al., 2011). The reduced phosphorylation observed in the present study has been detected using a traditional biochemical approach that does not allowed to conclude about the identity of the cell-types (MSNs vs TANs) in which this decrease occurs. However, given the small number of TANs in the striatum (1–2%, (Tepper and Bolam, 2004; Wilson et al., 1990) and the strong decrease in L-DOPA-induced signaling phosphorylation observed in VGLUT3 KO mice, it is reasonable to assume that these modifications

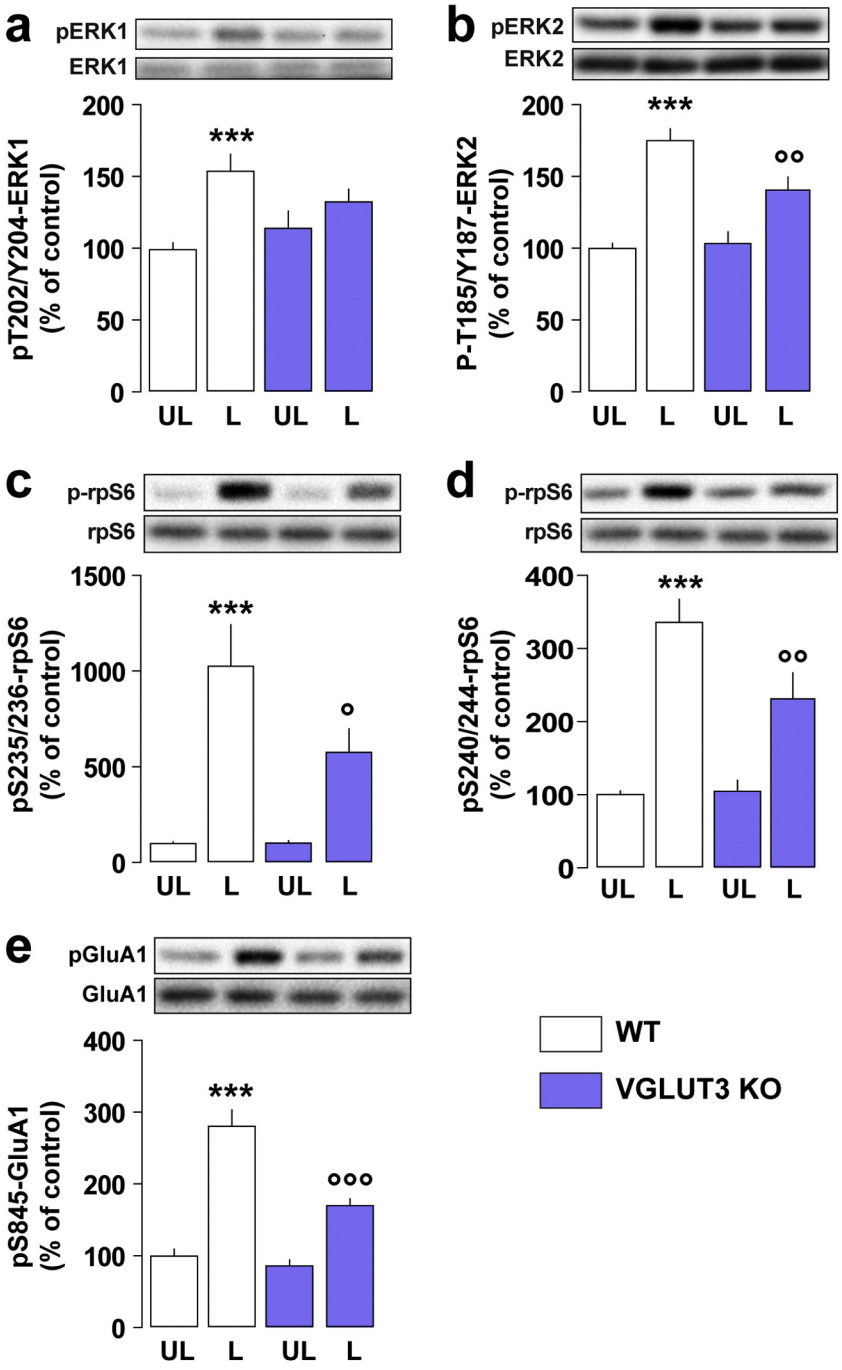

Fig. 7. Intracellular signaling pathways induced by L-DOPA are dampened in VGLUT3-deficient mice. Representative autoradiograms and quantifications of phosphorylated and total forms of ERK1 (**a**), ERK2 (**b**), rpS6 (**c** and **d**) and GluA1 (**e**) in wild-type (WT) and VGLUT3 KO mice. One-way ANOVA: (n = 9–12 mice per group) pT202/Y204-ERK1 ($F_{(3, 41)} = 7.26$, $p < 0.001$), pT185/Y187-ERK2 ($F_{(3, 41)} = 24.39$, $p < 0.001$), pS235/236-rpS6 ($F_{(3, 41)} = 11.48$, $p < 0.001$), p240/244-rpS6 ($F_{(3, 41)} = 21.19$, $p < 0.001$), pS845-GluA1 S845 ($F_{(3, 41)} = 33.73$, $p < 0.001$). Newman–Keuls *post-hoc* test was used for specific comparisons: ***$p < 0.001$ (WT-lesioned vs WT-unlesioned); °°°$p < 0.001$, °°$p < 0.01$ and °$p < 0.05$ (KO-lesioned vs WT-lesioned).

may occur in MSNs. Future studies will be necessary to determine whether VGLUT3 inactivation affects the phosphorylation in MSNs or/and TANs.

Finally, our data clearly show that decreasing VGLUT3 expression or activity could be beneficial to the therapeutic efficiency of L-DOPA therapy, thus identifying the atypical glutamate transporter as an innovative and promising pharmacological target for striatum-related disorders.

Supplementary data to this article can be found online at http://dx.doi.org/10.1016/j.nbd.2015.12.010.

Conflict of interest

The authors declare no conflict of interest.

Acknowledgments

This work was supported by Inserm and grants from ATIP-Avenir (Inserm) to EV. *Équipe* FRM DEQ20130326486, FRC, Brain Canada Multi-Investigator Research Initiative (SEM, MAMP, VFP), INSERM, CNRS and UPMC to SEM. MAMP and VFP were funded by the Canadian

Institutes of Health Research (MOP 126000 and MOP 89919) and NSERC (402524-2013). MG received a Fellowship from the Heart & Stroke Foundation of Ontario. GG was partially supported by The Company of Biologists and Boehringer Ingelheim Fonds.

References

Albin, R.L., et al., 1989. The functional anatomy of basal ganglia disorders. Trends Neurosci. 12, 366–375.

Amilhon, B., et al., 2010. VGLUT3 (vesicular glutamate transporter type 3) contribution to the regulation of serotonergic transmission and anxiety. J. Neurosci. 30, 2198–2210.

Bastide, M.F., et al., 2015. Pathophysiology of L-dopa-induced motor and non-motor complications in Parkinson's disease. Prog. Neurobiol. 132, 96–168.

Bateup, H.S., et al., 2010. Distinct subclasses of medium spiny neurons differentially regulate striatal motor behaviors. Proc. Natl. Acad. Sci. U. S. A. 107, 14845–14850.

Bennett, B.D., Wilson, C.J., 1999. Spontaneous activity of neostriatal cholinergic interneurons in vitro. J. Neurosci. 19, 5586–5596.

Bezard, E., Carta, M., 2015. Could the serotonin theory give rise to a treatment for levodopa-induced dyskinesia in Parkinson's disease? Brain 138, 829–830.

Bezard, E., et al., 2014. The mGluR5 negative allosteric modulator dipraglurant reduces dyskinesia in the MPTP macaque model. Mov. Disord. 29, 1074–1079.

Bonsi, P., et al., 2011. Centrality of Striatal cholinergic transmission in basal ganglia function. Front. Neuroanat. 5, 6.

Cachope, R., et al., 2012. Selective activation of cholinergic interneurons enhances accumbal phasic dopamine release: setting the tone for reward processing. Cell Rep. 2, 33–41.

Calabresi, P., et al., 2006. A convergent model for cognitive dysfunctions in Parkinson's disease: the critical dopamine-acetylcholine synaptic balance. Lancet Neurol. 5, 974–983.

Calabresi, P., et al., 2014. Direct and indirect pathways of basal ganglia: a critical reappraisal. Nat. Neurosci. 17, 1022–1030.

Carta, M., et al., 2007. Dopamine released from 5-HT terminals is the cause of L-DOPA-induced dyskinesia in Parkinsonian rats. Brain 130, 1819–1833.

Carta, M., et al., 2010. Role of serotonin neurons in the induction of levodopa- and graft-induced dyskinesias in Parkinson's disease. Mov. Disord. 25 (Suppl. 1), S174–S179.

Cenci, M.A., 2014. Presynaptic mechanisms of l-DOPA-induced dyskinesia: the findings, the debate, and the therapeutic implications. Front. Neurol. 5, 242.

Cenci, M.A., et al., 1998. L-DOPA-induced dyskinesia in the rat is associated with striatal overexpression of prodynorphin- and glutamic acid decarboxylase mRNA. Eur. J. Neurosci. 10, 2694–2706.

Centonze, D., et al., 2003. Receptor subtypes involved in the presynaptic and postsynaptic actions of dopamine on striatal interneurons. J. Neurosci. 23, 6245–6254.

Cerovic, M., et al., 2013. Molecular and cellular mechanisms of dopamine-mediated behavioral plasticity in the striatum. Neurobiol. Learn. Mem. 105, 63–80.

Chuhma, N., et al., 2014. Dopamine neurons control striatal cholinergic neurons via regionally heterogeneous dopamine and glutamate signaling. Neuron 81, 901–912.

Darmopil, S., et al., 2009. Genetic inactivation of dopamine D1 but not D2 receptors inhibits L-DOPA-induced dyskinesia and histone activation. Biol. Psychiatry 66, 603–613.

Day, M., et al., 2008. Differential excitability and modulation of striatal medium spiny neuron dendrites. J. Neurosci. 28, 11603–11614.

DeBoer, P., et al., 1993. Differential effect of systemic administration of bromocriptine and L-dopa on the release of acetylcholine from striatum of intact and 6-OHDA-treated rats. Brain Res. 608, 198–203.

Deffains, M., Bergman, H., 2015. Striatal cholinergic interneurons and cortico-striatal synaptic plasticity in health and disease. Mov. Disord. 30, 1014–1025.

Ding, J., et al., 2006. RGS4-dependent attenuation of M4 autoreceptor function in striatal cholinergic interneurons following dopamine depletion. Nat. Neurosci. 9, 832–842.

Ding, Y., et al., 2011. Enhanced striatal cholinergic neuronal activity mediates L-DOPA-induced dyskinesia in Parkinsonian mice. Proc. Natl. Acad. Sci. U. S. A. 108, 840–845.

Divito, C.B., et al., 2015. Loss of VGLUT3 produces circadian-dependent hyperdopaminergia and ameliorates motor dysfunction and l-Dopa-mediated dyskinesias in a model of Parkinson's disease. J. Neurosci. 35, 14983–14999.

Ehringer, H., Hornykiewicz, O., 1960. Distribution of noradrenaline and dopamine (3-hydroxytyramine) in the human brain and their behavior in diseases of the extrapyramidal system. Klin. Wochenschr. 38, 1236–1239.

El Mestikawy, S., et al., 2011. From glutamate co-release to vesicular synergy: vesicular glutamate transporters. Nat. Rev. Neurosci. 12, 204–216.

Espadas, I., et al., 2012. L-DOPA-induced increase in TH-immunoreactive striatal neurons in Parkinsonian mice: insights into regulation and function. Neurobiol. Dis. 48, 271–281.

Fahn, S., et al., 2004. Levodopa and the progression of Parkinson's disease. N. Engl. J. Med. 351, 2498–2508.

Feyder, M., et al., 2011. L-DOPA-induced dyskinesia and abnormal signaling in striatal medium spiny neurons: focus on dopamine D1 receptor-mediated transmission. Front. Behav. Neurosci. 5, 71.

Fieblinger, T., et al., 2014a. Cell type-specific plasticity of striatal projection neurons in Parkinsonism and L-DOPA-induced dyskinesia. Nat. Commun. 5, 5316.

Fieblinger, T., et al., 2014b. Mechanisms of dopamine D1 receptor-mediated ERK1/2 activation in the Parkinsonian striatum and their modulation by metabotropic glutamate receptor type 5. J. Neurosci. 34, 4728–4740.

Fino, E., et al., 2008. Cell-specific spike-timing-dependent plasticity in GABAergic and cholinergic interneurons in corticostriatal rat brain slices. J. Physiol. 586, 265–282.

Francardo, V., et al., 2011. Impact of the lesion procedure on the profiles of motor impairment and molecular responsiveness to L-DOPA in the 6-hydroxydopamine mouse model of Parkinson's disease. Neurobiol. Dis. 42, 327–340.

Franklin, K., Paxinos, G., 2007. The Mouse Brain in Stereotaxic Coordinates.

Fulceri, F., et al., 2006. Nigrostriatal damage with 6-OHDA: validation of routinely applied procedures. Ann. N. Y. Acad. Sci. 1074, 344–348.

Gagnon, D., Parent, M., 2013. Distribution of VGLUT3 in highly collateralized axons from the rat dorsal raphe nucleus as revealed by single-neuron reconstructions. PLoS One 9, e87709.

Gangarossa, G., Valjent, E., 2012. Regulation of the ERK pathway in the dentate gyrus by in vivo dopamine D1 receptor stimulation requires glutamatergic transmission. Neuropharmacology 63, 1107–1117.

Gangarossa, G., et al., 2013. Combinatorial topography and cell-type specific regulation of the ERK pathway by dopaminergic agonists in the mouse striatum. Brain Struct. Funct. 218, 405–419.

Gangarossa, G., et al., 2014a. Repeated stimulation of dopamine D1-like receptor and hyperactivation of mTOR signaling lead to generalized seizures, altered dentate gyrus plasticity, and memory deficits. Hippocampus 24, 1466–1481.

Gangarossa, G., et al., 2014b. T-type calcium channel Cav3.2 deficient mice show elevated anxiety, impaired memory and reduced sensitivity to psychostimulants. Front. Behav. Neurosci. 8, 92.

Girasole, A.E., Nelson, A.B., 2015. Probing striatal microcircuitry to understand the functional role of cholinergic interneurons. Mov. Disord. 30, 1306–1318.

Gras, C., et al., 2002. A third vesicular glutamate transporter expressed by cholinergic and serotoninergic neurons. J. Neurosci. 22, 5442–5451.

Gras, C., et al., 2008. The vesicular glutamate transporter VGLUT3 synergizes striatal acetylcholine tone. Nat. Neurosci. 11, 292–300.

Guzman, M.S., et al., 2011. Elimination of the vesicular acetylcholine transporter in the striatum reveals regulation of behaviour by cholinergic–glutamatergic co-transmission. PLoS Biol. 9, e1001194.

Heiman, M., et al., 2014. Molecular adaptations of striatal spiny projection neurons during levodopa-induced dyskinesia. Proc. Natl. Acad. Sci. U. S. A. 111, 4578–4583.

Herzog, E., et al., 2004. Localization of VGLUT3, the vesicular glutamate transporter type 3, in the rat brain. Neuroscience 123, 983–1002.

Higley, M.J., et al., 2011. Cholinergic interneurons mediate fast VGluT3-dependent glutamatergic transmission in the striatum. PLoS One 6, e19155.

Iderberg, H., et al., 2013. Modulating mGluR5 and 5-HT1A/1B receptors to treat l-DOPA-induced dyskinesia: effects of combined treatment and possible mechanisms of action. Exp. Neurol. 250, 116–124.

Kannari, K., et al., 2001. Activation of 5-HT(1A) but not 5-HT(1B) receptors attenuates an increase in extracellular dopamine derived from exogenously administered L-DOPA in the striatum with nigrostriatal denervation. J. Neurochem. 76, 1346–1353.

Kayadjanian, N., et al., 1999. Cortical and nigral deafferentation and striatal cholinergic markers in the rat dorsal striatum: different effects on the expression of mRNAs encoding choline acetyltransferase and muscarinic m1 and m4 receptors. Eur. J Neurosci. 11, 3659–3668.

Kravitz, A.V., et al., 2010. Regulation of Parkinsonian motor behaviours by optogenetic control of basal ganglia circuitry. Nature 466, 622–626.

Lim, S.A., et al., 2014. Striatal cholinergic interneuron regulation and circuit effects. Front. Synaptic Neurosci. 6, 22.

Lindgren, H.S., et al., 2009. Differential involvement of D1 and D2 dopamine receptors in L-DOPA-induced angiogenic activity in a rat model of Parkinson's disease. Neuropsychopharmacology 34, 2477–2488.

Lundblad, M., et al., 2002. Pharmacological validation of behavioural measures of akinesia and dyskinesia in a rat model of Parkinson's disease. Eur. J. Neurosci. 15, 120–132.

Lundblad, M., et al., 2004. A model of L-DOPA-induced dyskinesia in 6-hydroxydopamine lesioned mice: relation to motor and cellular parameters of nigrostriatal function. Neurobiol. Dis. 16, 110–123.

Mallet, N., et al., 2006. Cortical inputs and GABA interneurons imbalance projection neurons in the striatum of Parkinsonian rats. J. Neurosci. 26, 3875–3884.

Maurice, N., et al., 2004. D2 dopamine receptor-mediated modulation of voltage-dependent Na + channels reduces autonomous activity in striatal cholinergic interneurons. J. Neurosci. 24, 10289–10301.

Morin, N., et al., 2013. Chronic treatment with MPEP, an mGlu5 receptor antagonist, normalizes basal ganglia glutamate neurotransmission in L-DOPA-treated Parkinsonian monkeys. Neuropharmacology 73, 216–231.

Morin, N., et al., 2014. Effect of a chronic treatment with an mGlu5 receptor antagonist on brain serotonin markers in Parkinsonian monkeys. Prog. Neuro-Psychopharmacol. Biol. Psychiatry 56, 27–38.

Murer, M.G., Moratalla, R., 2011. Striatal signaling in L-DOPA-induced dyskinesia: common mechanisms with drug abuse and long term memory involving D1 dopamine receptor stimulation. Front. Neuroanat. 5, 51.

Nahimi, A., et al., 2012. Serotonergic modulation of receptor occupancy in rats treated with L-DOPA after unilateral 6-OHDA lesioning. J. Neurochem. 120, 806–817.

Nelson, A.B., et al., 2014. Striatal cholinergic neurotransmission requires VGLUT3. J. Neurosci. 34, 8772–8777.

Ouattara, B., et al., 2011. Metabotropic glutamate receptor type 5 in levodopa-induced motor complications. Neurobiol. Aging 32, 1286–1295.

Pavon, N., et al., 2006. ERK phosphorylation and FosB expression are associated with L-DOPA-induced dyskinesia in hemiparkinsonian mice. Biol. Psychiatry 59, 64–74.

Picconi, B., Calabresi, P., 2014. Targeting metabotropic glutamate receptors as a new strategy against levodopa-induced dyskinesia in Parkinson's disease? Mov. Disord. 29, 715–719.

Picconi, B., et al., 2003. Loss of bidirectional striatal synaptic plasticity in L-DOPA-induced dyskinesia. Nat. Neurosci. 6, 501–506.

Pisani, A., et al., 2003. Targeting striatal cholinergic interneurons in Parkinson's disease: focus on metabotropic glutamate receptors. Neuropharmacology 45, 45–56.
Pisani, A., et al., 2007. Re-emergence of striatal cholinergic interneurons in movement disorders. Trends Neurosci. 30, 545–553.
Rylander, D., et al., 2010. Maladaptive plasticity of serotonin axon terminals in levodopa-induced dyskinesia. Ann. Neurol. 68, 619–628.
Sakae, D.Y., et al., 2015. The absence of VGLUT3 predisposes to cocaine abuse by increasing dopamine and glutamate signaling in the nucleus accumbens. Mol. Psychiatry 20, 1448–1459.
Santini, E., et al., 2007. Critical involvement of cAMP/DARPP-32 and extracellular signal-regulated protein kinase signaling in L-DOPA-induced dyskinesia. J. Neurosci. 27, 6995–7005.
Santini, E., et al., 2009a. L-DOPA activates ERK signaling and phosphorylates histone H3 in the striatonigral medium spiny neurons of hemiparkinsonian mice. J. Neurochem. 108, 621–633.
Santini, E., et al., 2009b. Inhibition of mTOR signaling in Parkinson's disease prevents L-DOPA-induced dyskinesia. Sci. Signal. 2, ra36.
Santini, E., et al., 2012. Dopamine- and cAMP-regulated phosphoprotein of 32-kDa (DARPP-32)-dependent activation of extracellular signal-regulated kinase (ERK) and mammalian target of rapamycin complex 1 (mTORC1) signaling in experimental parkinsonism. J. Biol. Chem. 287, 27806–27812.
Stensrud, M.J., et al., 2013. Vesicular glutamate transporter-3 in the rodent brain: vesicular colocalization with vesicular gamma-aminobutyric acid transporter. J. Comp. Neurol. 521, 3042–3056.
Tepper, J.M., Bolam, J.P., 2004. Functional diversity and specificity of neostriatal interneurons. Curr. Opin. Neurobiol. 14, 685–692.
Thiele, S.L., et al., 2014. Selective loss of bi-directional synaptic plasticity in the direct and indirect striatal output pathways accompanies generation of parkinsonism and l-DOPA induced dyskinesia in mouse models. Neurobiol. Dis. 71, 334–344.
Tozzi, A., et al., 2011. The distinct role of medium spiny neurons and cholinergic interneurons in the D(2)/A(2)A receptor interaction in the striatum: implications for Parkinson's disease. J. Neurosci. 31, 1850–1862.
Westin, J.E., et al., 2007. Spatiotemporal pattern of striatal ERK1/2 phosphorylation in a rat model of L-DOPA-induced dyskinesia and the role of dopamine D1 receptors. Biol. Psychiatry 62, 800–810.
Wilson, C.J., et al., 1990. Firing patterns and synaptic potentials of identified giant aspiny interneurons in the rat neostriatum. J. Neurosci. 10, 508–519.
Won, L., et al., 2014. Striatal cholinergic cell ablation attenuates L-DOPA induced dyskinesia in Parkinsonian mice. J. Neurosci. 34, 3090–3094.